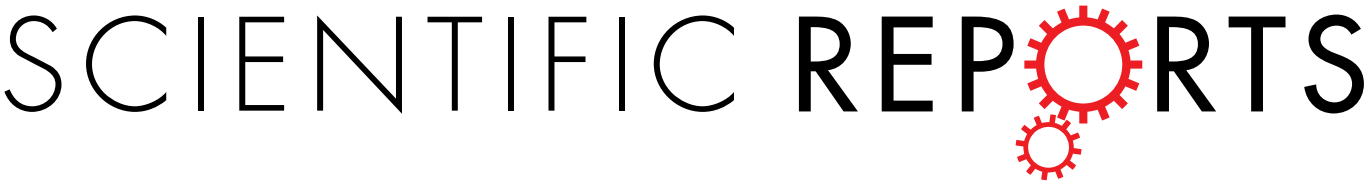

OPEN

Theoretical study of superionic phase transition in Li_2S

Sara Panahian Jand, Qian Zhang & Payam Kaghazchi

Received: 30 January 2017
Accepted: 2 June 2017
Published online: 19 July 2017

We have studied temperature-induced superionic phase transition in Li_2S, which is one of the most promising Li-S battery cathode material. Concentration of ionic carriers at low and high temperature was evaluated from thermodynamics of defects (using density functional theory) and detailed balance condition (using *ab initio* molecular dynamics (AIMD)), respectively. Diffusion coefficients were also obtained using AIMD simulations. Calculated ionic conductivity shows that superionic phase transition occurs at $T = 900$ K, which is in agreement with reported experimental values. The superionic behavior of Li_2S is found to be due to thermodynamic reason (i.e. a large concentration of disordered defects).

Ionic conductivity of electrode and electrolyte materials is an important parameter for the operation of Li-based batteries. Mechanism and rate of Li diffusion through Li-based battery materials have therefore been studied extensively[1–4]. In addition, different strategies have been proposed to increase carrier concentration and mobility (i.e. improving Li ion conductivity) in solid state materials[2,5,6]. Moreover, superionic compounds are widely investigated because of their fundamental interests and potential applications in solid-state batteries, fuel cells, and gas sensors[7–12]. These ionic crystals have high ionic conductivity at temperatures below the melting point. Above the temperature of superionic phase transition one of the ion sublattices becomes disordered leading to a high ionic conductivity. Extensive experimental and theoretical studies have been carried out to understand the structure and diffusion behaviour of superionic compounds. Experimental neutron diffraction[13–16] and theoretical molecular dynamics (MD)[17–20] are the most commonly used techniques to investigate these materials. Li-based compounds are of special interests due to their applications in Li-based batteries. In particular, Li_2S is one of the most promising Li-S battery cathode materials. Ionic conductivity of Li_2S is a key factor determining the performance of Li-S batteries. Li_2S is also interesting from scientific point of view as it is a supersonic conductor at temperatures higher than ≈900 K[21]. The ionic conductivity of Li_2S has been measured to be 1.27×10^{-1} S/cm at 1170 K[22]. The quasielastic neutron scattering study by Altorfer *et al.*[22] proposed two models for Li transport in the superionic phase of Li_2S: (i) Li vacancy jumps between regular Li sites and (ii) Li jumps between regular Li and interstitial defective sites. In spite of the importance of Li-S batteries, temperature-dependent Li ion conductivity in Li_2S has not been theoretically studied so far. In this work, we combine *ab initio* molecular dynamics (AIMD) and density functional theory (DFT) as well as thermodynamic and kinetic considerations to calculate Li ion conductivity as function of temperature and apply this approach to study the mechanism of superionic phase transition in Li_2S.

To evaluate diffusion coefficients, 50 ps AIMD simulations (see Method part for further details) were carried out for pristine Li_2S and Li_2S with a single vacancy at temperatures $T = 300$, 600, 750, 830, 900, 1050, 1170, and 1300 K. The thermalization was achieved within 10 ps and the rest 40 ps were used for structure sampling. Note that it is very important to perform the AIMD simulation without considering any symmetry constraint. Total mean square displacements of Li ions as function of lag time (MSD(τ)) for Li_2S (modelled using $2 \times 2 \times 2$ unit cells) with a single Li vacancy at different temperatures are illustrated in Fig. 1. Only few number of Li vacancy hoppings were observed for $T = 300$, 600, and 750 K. Therefore we have not considered these temperatures in Fig. 1. For higher temperatures, we have observed more than 32 jumps in Li_2S (modelled with a $2 \times 2 \times 2$ unit cell) during 40 ps AIMD simulation which is expected to be sufficient for our analysis. Calculated diffusion coefficients of Li in Li_2S with one Li vacancy using the Einstein relation (D) indicate a change in slope at 1050 K (see Fig. 1), showing that Li diffusion occurs via a mechanism distinct from the Li vacancy hopping at high temperatures.

To uncover the mechanism of Li diffusion at high temperatures, we extracted visited positions of Li and S ions within the $\{1\bar{1}0\}$ planes of Li_2S with a single Li vacancy at different temperatures (Fig. 2). It is found that Li transport occurs mainly via Li vacancy hopping between regular Li sites (so called 8c sites) at low temperatures such as $T = 830$ K. At higher temperatures anharmonic elongation in Li ion positions appear. Although Li transport still takes place mainly via Li vacancy hopping between 8c sites, there are few Li jumps between 8c and interstitial

Institut für Chemie und Biochemie, Freie Universität Berlin, Takustr, 3, 14195, Berlin, Germany. Correspondence and requests for materials should be addressed to P.K. (email: payam.kaghazchi@fu-berlin.de)

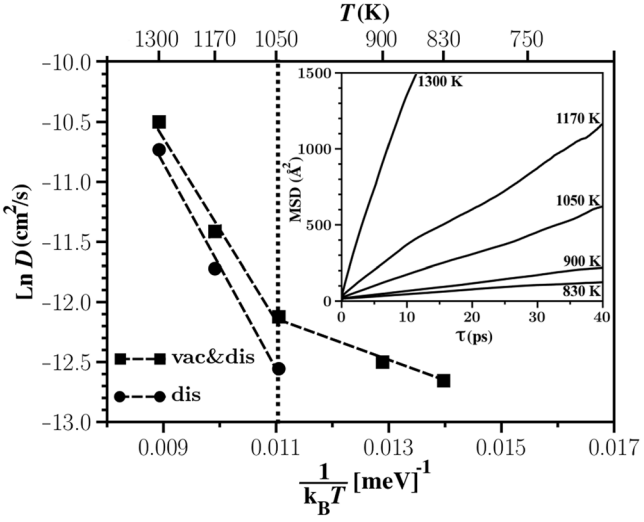

Figure 1. Arrhenius plot of diffusion coefficients in Li_2S. Diffusion coefficient in the pristine structure is shown by D_{dis} since in this case Li ion migration takes place via temperature–induced disorder (interstitial Li). Li diffusion in Li_2S with a single vacancy is illustrated by vac&dis as charge carriers are both Li vacancy and disorder (interstitial Li). The inset presents total mean square displacements (MSD) versus lag time calculated for 40 ps AIMD simulations.

defective sites (so called 4b sites) at $T = 900$ K. At $T = 1050$ K, Li transport is due to both –8c–8c–8c– and –8c–4b–8c– mechanisms. However, Li diffusion at 1170 K and 1300 K is mainly along the latter pathway. The only possible mechanism for Li migration at low temperatures is the vacancy hopping, and D_{vac} is calculated directly from the Einstein relation. D_{vac} for temperatures higher than 1050 K is obtained by extrapolating the low temperature values of D_{vac} (see Fig. 1). At 1170 K, the value of D for diffusion of Li along –8c–4b–8c– (D_{dis}) is larger than the value of D for diffusion of Li along –8c–8c–8c– (D_{vac}). Li diffusion takes place only through –8c–4b–8c– pathway in pristine structure ($D_{pris} = D_{dis}$). For this reason, diffusion coefficient in pristine Li_2S (modelled using $2 \times 2 \times 2$ unit cells) D_{pris} at 1170 K and 1300 K is close to that in Li_2S with a single vacancy. The calculated value of $D_{vac\&dis} = 1.03 \times 10^{-5}$ cm^2/s at 1170 K (superionic regime), which includes diffusion of Li along both –8c–8c–8c– and –8c–4b–8c– pathways, is in agreement with the experimental value of 1.39×10^{-5} cm^2/s[22]. However, at this temperature the value of D for diffusion of Li along –8c–4b–8c– (D_{dis}) is only 1.2 times larger than the value of D for diffusion of Li along –8c–8c–8c– (i.e. extrapolated value of D_{vac} from the low temperature regime). Therefore, the superionic behavior of Li_2S is not due to kinetic reason.

To determine the most probable defect types and their concentrations (thermodynamic factor of ionic conductivity) in poor-ionic conductor phase, we need to obtain the formation energy of defects ($\Delta E_d^{i,q}$). Recently, we have calculated $\Delta E_d^{i,q}$ for a variety of possible defects in poor ionic conductor phase of Li_2S[23] and found that charged interstitial Li (Li^+) and Li vacancy (V_{Li}^-) are the most favorable ionic charge carriers[23]. However, we have recently found that the values of $\Delta E_d^{i,q}$ depend strongly on several computational parameters such as unit cell size and the value of dielectric constant (ϵ) that is used to correct the finite-cell size effect of charged defects and align the electrostatic potentials of defective and pristine supercells (ΔE). In this work, we recalculate $\Delta E_d^{i,q}$ using optimal parameters. Defect formation energies are calculated by

$$\Delta E_d^{i,q} = E_{tot}^{i,q} - E_{tot}^{Li_2S} + \sum_i n_i \mu_i + q(\epsilon_F + \epsilon_{VBM}) + \Delta E. \quad (1)$$

Here, $E_{tot}^{i,q}$ and $E_{tot}^{Li_2S}$ are the total energies of defective and pristine Li_2S, which have been calculated using DFT calculations (see Method part for further details). n_i and μ_i are the number and chemical potential of defects (Li or S). In our previous work, we used the electronic ϵ (ϵ_{el}) calculated by density functional perturbation theory (DFPT)[23]. The value of ϵ_{el} is generally smaller than the experimental value of static (low-frequency) ϵ (ϵ_s). The value of ϵ_s for Li_2S at room temperature has been estimated by Yang *et al.*[24] to be around 10, which is almost 3 times larger than our ϵ_{el} value obtained from the DFPT method. In the present work, we use the value of $\epsilon_s \approx 10$ to calculate ΔE. Moreover, instead of using a $2 \times 2 \times 2$ unit cell which was applied in our previous work[23], we use a $3 \times 3 \times 3$ unit cell to calculate the total energies. μ_{Li} is considered to be smaller than the total energy per atom of bulk metal Li (E_{tot}^{Li}). Moreover, it can not be smaller than a μ_{Li} value at which Li_2S decomposes. By defining $\Delta\mu_{Li}$ to be $\mu_{Li} - E_{tot}^{Li}$ the permitted range of $\Delta\mu_{Li}$ is between 0 and half of the Gibbs energy of formation of Li_2S.

To calculate $\Delta E_d^{i,q}$ and ϵ_F as function of $\Delta\mu_{Li}$, we consider the requirement of charge neutrality

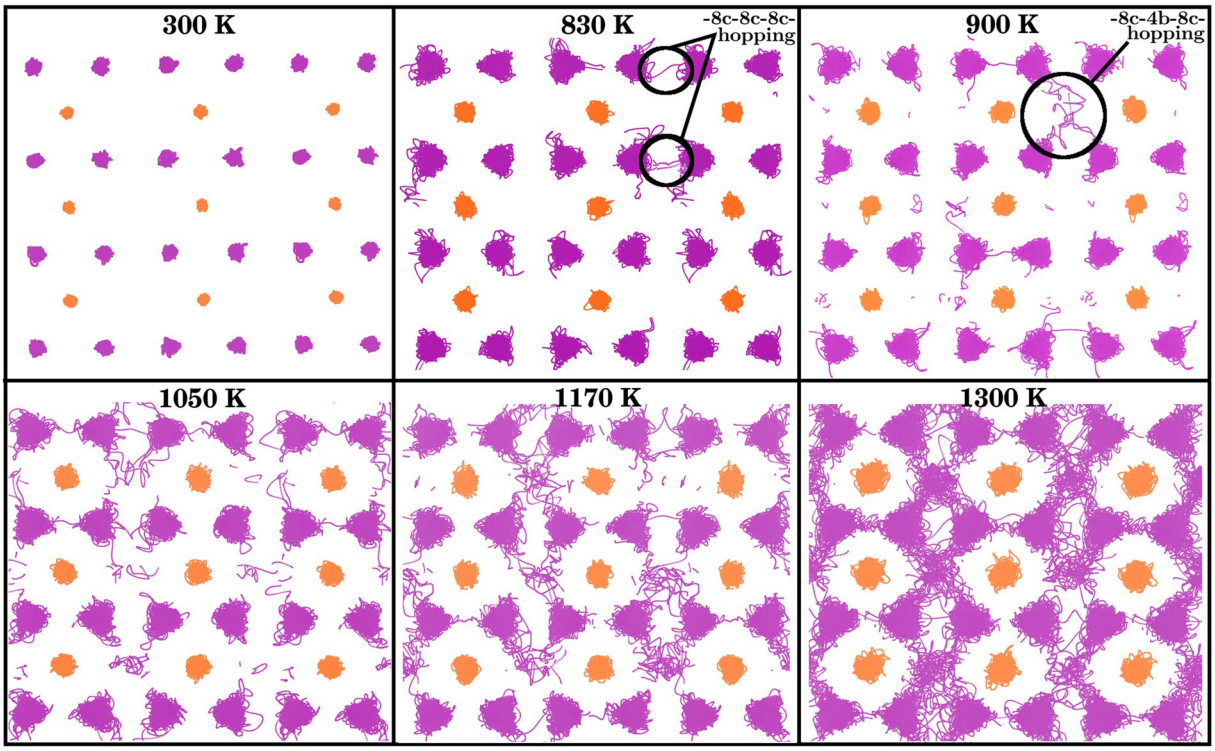

Figure 2. Visited Li and S ion positions in the $\{1\bar{1}0\}$ planes of Li_2S within slices of 1.7 Å thickness during 40 ps of AIMD simulations at 300 K, 830 K, 900 K, 1050 K, 1170 K and 1300 K. The visited positions by Li and S ions are in purple and gold, respectively.

$$\underbrace{\int_{\mathrm{CBM}}^{\infty} D(\epsilon) f(\epsilon,\, \epsilon_{\mathrm{F}}) d\varepsilon}_{n_{\mathrm{e}}} - \underbrace{\int_{-\infty}^{\mathrm{VBM}} D(\epsilon)[1 - f(\epsilon,\, \epsilon_{\mathrm{F}})] d\epsilon}_{n_{\mathrm{h}}} = \sum_i q_i \underbrace{n_i^0 \exp\left(-\frac{\Delta E_{\mathrm{d}}^{i,q}}{k_B T}\right)}_{n_i}. \tag{2}$$

In this equation, $D(\epsilon)$ is the density of states, $f(\epsilon, \epsilon_{\mathrm{F}})$ is the Fermi-Dirac distribution, q_i is the charge state of defect i. n_{e}, n_{h}, and n_{i} are the concentration of electrons, holes, and defects of type i, while n_i^0 is the maximum possible concentration of defects of type i per unit volume. Since eqs (1) and (2) are self-consistent, $\Delta E_{\mathrm{d}}^{i,q}$ and ϵ_F are calculated iteratively.

Figure 3 shows that for $-2.0\,\mathrm{eV} < \Delta\mu_{\mathrm{Li}} \leq 0\,\mathrm{eV}$ the formation energy of Li^- vacancy ($\Delta E_{\mathrm{d}}^{V_{\mathrm{Li}}^-}$) is 0.80 eV, which is 0.22 eV lower than the $\Delta E_{\mathrm{d}}^{V_{\mathrm{Li}}^-}$ value calculated for $\epsilon_{\mathrm{e}} \approx 3.6$ and $2 \times 2 \times 2$ unit cells. The formation energy of Li^+ interstitial ($\Delta E_{\mathrm{d}}^{\mathrm{Li}^+}$) is very similar to $\Delta E_{\mathrm{d}}^{V_{\mathrm{Li}}^-}$. Therefore, for $-2.0\,\mathrm{eV} < \Delta\mu_{\mathrm{Li}} \leq 0\,\mathrm{eV}$ ionic transport in Li_2S occurs via formation of Frenkel $V_{\mathrm{Li}}^- + \mathrm{Li}^+$ pairs and their diffusion.

Figure 3 also demonstrates that for $-2.3\,\mathrm{eV} \leq \Delta\mu_{\mathrm{Li}} \leq -2.0\,\mathrm{eV}$ the value of $\Delta E_{\mathrm{d}}^{V_{\mathrm{Li}}^-}$ decreases, while $\Delta E_{\mathrm{d}}^{\mathrm{Li}^+}$ increases. At this range of $\Delta\mu_{\mathrm{Li}}$ the Fermi level shifts toward the valence band maximum leading to the increase of concentration of holes. Under this condition, the ionic conductivity takes place via formation and diffusion of V_{Li}^-. The calculated value of diffusion barrier for V_{Li}^- and Li^+ from DFT-NEB calculations[23] are $\Delta E_{\mathrm{b}}^{V_{\mathrm{Li}}^-} = 0.27\,\mathrm{eV}$ and $\Delta E_{\mathrm{b}}^{\mathrm{Li}^+} = 0.45\,\mathrm{eV}$, respectively. The activation energy of Li transport via the Frenkel mechanism is $\Delta E_{\mathrm{d}}^{V_{\mathrm{Li}}^-} + \Delta E_{\mathrm{d}}^{\mathrm{Li}^+} + \Delta E_{\mathrm{b}}^{V_{\mathrm{Li}}^-} = 1.8\,\mathrm{eV}$ for $-2.0\,\mathrm{eV} < \Delta\mu_{\mathrm{Li}} \leq 0\,\mathrm{eV}$. However, the minimum value of activation energy is for the creation and diffusion of Li vacancy: $\Delta E_{\mathrm{d}}^{V_{\mathrm{Li}}^-} + \Delta E_{\mathrm{b}}^{V_{\mathrm{Li}}^-} = 0.95\,\mathrm{eV}$ at $\Delta\mu_{\mathrm{Li}} = -2.3\,\mathrm{eV}$. Afterwards, we calculated the concentration of Li vacancy as function of chemical potential of Li (Fig. 3). We can distinguish two regimes for the concentration of Li: (i) low concentration regime for $-2.0\,\mathrm{eV} < \Delta\mu_{\mathrm{Li}} \leq 0\,\mathrm{eV}$ with $c' = 2.8 \times 10^9\,\mathrm{cm}^{-3}$ and (ii) high concentration regime for $-2.3\,\mathrm{eV} \leq \Delta\mu_{\mathrm{Li}} \leq -2.0\,\mathrm{eV}$ with maximum $c = 3.5 \times 10^{11}\,\mathrm{cm}^{-3}$. To calculate conductivity as function of temperature we will consider c' and c.

Figure 4 illustrates calculated concentration of V_{Li}^-, namely (n_{vac}), at $\Delta\mu_{\mathrm{Li}} = -2.3\,\mathrm{eV}$ at different temperatures using eq. (2). To estimate the concentration of Li at 4b sites in the superionic phase we used the detailed balance condition

$$n_{\mathrm{dis}} = \frac{n_{\mathrm{Li(8c)}}}{1 + \frac{\tau_{8c}}{\tau_{4b}}}, \tag{3}$$

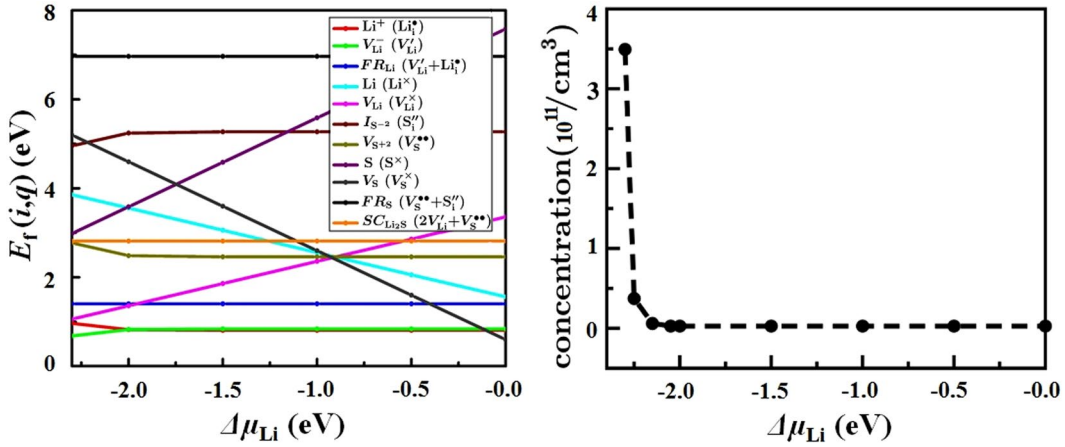

Figure 3. (left) Formation energies of different types of defects in bulk Li_2S as function of $\Delta\mu_{Li}$ (chemical potential of Li). Kroger–Vink representations are given in parentheses. (right) Concentration of Li vacancy as function of $\Delta\mu_{Li}$.

where $n_{Li(8c)}$ is the concentration of regular sites (4.27×10^{22} cm^{-3} for the theoretical lattice constant of 5.72 Å). τ_{4b} and τ_{8c} are the residence time for Li at 4b and 8c sites during AIMD simulations between 10 ps and 50 ps. The calculated values of n_{dis} for $T = 830$, 900, 1050, 1170 and 1300 K are illustrated in Fig. 4. We find that at 1300 K the concentration of 4b defect in the superionic phase is 48.6 times larger than the maximum possible concentration of V_{Li}^- (at $\Delta\mu_{Li} = -2.3$ eV) in poor-ionic conductor phase of Li_2S.

Finally, the ionic conductivity as function of temperature is determined by

$$\sigma_{tot} = \sigma_{vac} + \sigma_{dis} = \frac{q^2F^2}{RT}[n_{vac}D_{vac} + n_{dis}D_{dis}]. \quad (4)$$

where q, F, R, and T are charge of the carrier, Faraday constant, gas constant, and temperature, respectively. Calculated σ as function of temperature for two different concentration regimes is illustrated in Fig. 4. We find a clear superionic phase transition approximately at 900 K in the case of high concentration regime, which is in fair agreement with the Neutron scattering measurements by Altorfer *et al.*[22] and Buehrer *et al.*[21] showing that the superionic phase transition in Li_2S takes place near 800 K and 900 K, respectively. Since phase transition at 900 K in the case of low–concentration regime is not very apparent, we will not discuss this case further. According to the Arrhenius plot of diffusion coefficients (see Fig. 1) the superionic phase transition starts at $T = 1050$ K, which is larger than $T = 900$ K at which disorder starts to form according to Figs 2 and 4. The value of σ at 300 K (9.43×10^{-17} S/cm) is very small, which is in agreement with the general belief that the value of σ for Li_2S under ambient condition is very low. We are not aware of any experimental study measuring σ at 300 K.

The calculated value of σ at 1170 K is 3.02×10^{-2} S/cm, which is 4.2 times smaller than the experimental value of $\approx 1.27 \times 10^{-1}$ S/cm (estimated from the conductivity versus temperature curve in ref. 22). The difference between experimental and theoretical values of σ might be because of (i) the underestimation of n_{dis} (needed for the calculation of σ in eq. (4)), which is due to the computational limitation for the AIMD simulations, as well as (ii) computational and experimental uncertainties. Finally, we find that the calculated values of $\sigma_{dis}/\sigma_{vac}$ at 900 K, 1170 K and 1300 K are 1.1, 47.1, and 138.9 respectively, showing that the enhancement of ionic conductivity in superionic regime is between one and two orders of magnitude depending on temperature.

In summary, we have combined AIMD and DFT calculations with thermodynamic and kinetic considerations to calculate diffusion coefficient, defect concentration, and ionic conductivity of Li_2S as function of temperature. We find that Li ion transport at low temperatures (e.g. $T = 830$ K) occurs via Li vacancy hopping between regular Li sites. At and above the temperature of superionic phase transition, namely $T = 900$ K, Li ion transport takes place via both Li vacancy hopping between regular Li sites and Li hopping between regular and interstitial sites. At higher temperatures the latter mechanism becomes dominant. The increase in the concentration of interstitial Li plays the dominant role in the superionic behavior. For this reason although the calculated Arrhenius plot shows that the transition temperature to the superionic state is 1050 K, the calculated ionic conductivity shows a phase transition at 900 K, which is in agreement with experimental measurements. The presented approach in this work can be used to study superionic phase transition in other ionic crystals.

Methods

DFT Calculations. The DFT calculations were performed using the projector-augmented plane-wave code VASP[25–28]. The bulk Li_2S was modelled by $3 \times 3 \times 3$ super cells with $2 \times 2 \times 2$ Monkhorst-Pack k-point mesh with an energy cutoff of 300 eV. We have calculated the electronic and atomic structures as well as defect formation energies using the generalized gradient approximation (GGA) exchange-correlation functional proposed by Perdew, Burke, and Ernzerhof (PBE)[29].

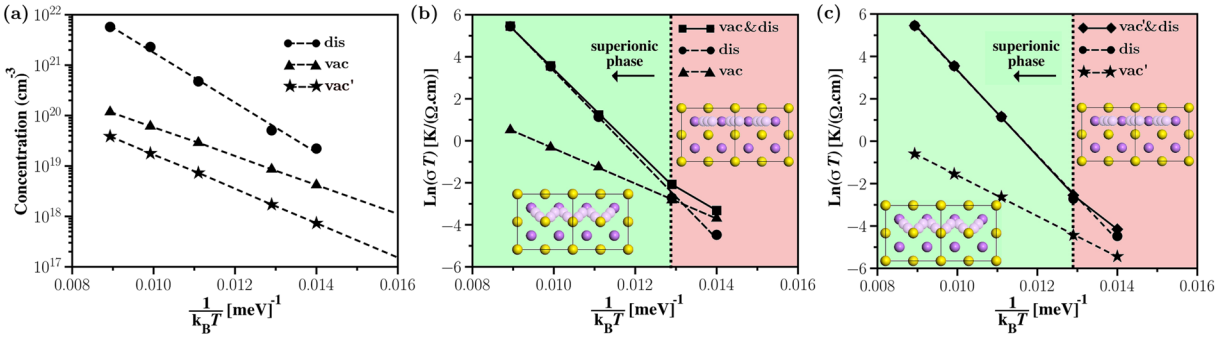

Figure 4. (**a**) Concentration of Li vacancy as function of temperature inverse calculated by eqs (1) and (2) for $-2.3\,\text{eV} \leq \Delta\mu_{Li} \leq -2.0\,\text{eV}$ (vac) and $-2.0\,\text{eV} < \Delta\mu_{Li} \leq 0\,\text{eV}$ (vac′) as well as that of interstitial Li calculated by eq. (3) (dis). Li ion conductivities as function of temperature inverse for (**b**) vac&dis and (**c**) vac′&dis.

AIMD Simulations. The diffusion pathway and diffusion coefficient were evaluated using the *ab initio* MD (AIMD) calculations (implemented in VASP). AIMD calculations were performed in the canonical (NVT) ensemble with time steps of 1 fs. Bulk Li_2S was modelled by $2 \times 2 \times 2$ super cells with $4 \times 4 \times 4$ Monkhorst-Pack *k*-point mesh with an energy cutoff of 360 eV. Mean Square Displacements (MSD) is obtained through the following equation:

$$\text{MSD}(\tau) = \frac{1}{N_{atom}} \frac{1}{N_{step} - \tau} \times \sum_{j=1}^{N_{atom}} \sum_{i=1}^{N_{step}-\tau} \left| \vec{r}_j(t_i + \tau) - \vec{r}_j(t_i) \right|^2, \tag{5}$$

where τ is lag time, N_{atom} and N_{step} are the number of diffusing Li ions and number of AIMD time steps (in our work 40000). Diffusion coefficient D is calculated using the Einstein relation:

$$D = \lim_{\tau \to \infty} \frac{\text{MSD}(\tau)}{6\tau}. \tag{6}$$

References

1. Shi, S. *et al*. Direct calculation of Li-ion transport in the solid electrolyte interphase. *Journal of the American Chemical Society* **134**, 15476–15487 (2012).
2. Yang, Y. *et al*. Elastic properties, defect thermodynamics, electrochemical window, phase stability, and Li^+ mobility of Li_3PS_4: Insights from first-principles calculations. *ACS Applied Materials & Interfaces* **8**, 25229–25242 (2016).
3. Gao, J., Zhao, Y. S., Shi, S. Q. & Li, H. Lithium–ion transport in inorganic solid state electrolyte, *Chinese Physics B* **25**, 018211 (2016).
4. Shi, S. *et al*. Multi-scale computation methods: Their applications in lithium-ion battery. *Chinese Physics B* **25**, 018212 (2016).
5. Shi, S., Qi, Y., Li, H. & Hector, L. G. Jr. Defect thermodynamics and diffusion mechanisms in Li_2CO_3 and implications for the solid electrolyte interphase in Li-ion batteries. *The Journal of Physical Chemistry C* **117**, 8579–8593 (2013).
6. Gao, J., Shi, S., Xiao, R. & Li, H. Synthesis and ionic transport mechanisms of α-$LiAlO_2$. *Solid State Ionics* **286**, 122–134 (2016).
7. Bruce, P. G. Solid-state chemistry of lithium power sources. *Chemical Communications* 1817–1824 (1997).
8. Tarascon, J.-M. & Armand, M. Issues and challenges facing rechargeable lithium batteries. *Nature* **414**, 359–367 (2001).
9. Minh, N. Q. Ceramic fuel cells. *Journal of the American Ceramic Society* **76**, 563–588 (1993).
10. Bonanos, N., Knight, K. & Ellis, B. Perovskite solid electrolytes: structure, transport properties and fuel cell applications. *Solid State Ionics* **79**, 161–170 (1995).
11. Carrette, L., Friedrich, K. A. & Stimming, U. Fuel cells: principles, types, fuels, and applications. *ChemPhysChem* **1**, 162–193 (2000).
12. Adachi, G.-y. & Imanaka, N. Rare earth contribution in solid state electrolytes, especially in the chemical sensor field. *Journal of Alloys and Compounds* **250**, 492–500 (1997).
13. Keen, D. & Hull, S. The high-temperature structural behaviour of copper (i) iodide. *Journal of Physics: Condensed Matter* **7**, 5793 (1995).
14. Hull, S. & Keen, D. Structural characterization of the superionic transition in Ag_2HgI_4 and Cu_2HgI_4. *Journal of Physics: Condensed Matter* **12**, 3751 (2000).
15. Keen, D. A. & Hull, S. Determination of structural disorder in superionic by neutron total scattering. *Journal of Physics: Condensed Matter* **10**, 8217 (1998).
16. Hull, S. Superionics: crystal structures and conduction processes. *Reports on Progress in Physics* **67**, 1233 (2004).
17. Wang, Y. *et al*. Design principles for solid-state lithium superionic conductors. *Nature Materials* (2015).
18. Mohn, C. E., Sølen, S. & Hull, S. Diffusion within α-cui studied using *ab-initio* molecular dynamics simulations. *Journal of Physics: Condensed Matter* **21**, 335403 (2009).
19. Keen, D. *et al*. Nature of the superionic transition in Ag^+ and Cu^+ halides. *Physical Review B* **68**, 014117 (2003).
20. Chu, I.-H. *et al*. Insights into the performance limits of the $Li_2P_3S_{11}$ superionic conductor: A combined first–principles and experimental study. *ACS Applied Materials & Interfaces* **8**, 7843–7853 (2016).
21. Buehrer, W. *et al*. Lattice dynamics and the diffuse phase transition of lithium sulphide investigated by coherent neutron scattering. *Journal of Physics: Condensed Matter* **3**, 1055 (1991).
22. Altorfer, F. *et al*. Lithium diffusion in the superionic conductor Li_2S. *Physica B: Condensed Matter* **180**, 795–797 (1992).
23. Moradabadi, A. & Kaghazchi, P. Thermodynamics and kinetics of defects in Li_2S. *Applied Physics Letters* **108**, 213906 (2016).
24. Yang, Y. *et al*. High-capacity micrometer-sized Li_2S particles as cathode materials for advanced rechargeable lithium-ion batteries. *Journal of the American Chemical Society* **134**, 15387–15394 (2012).
25. Kresse, G. & Hafner, J. *Ab initio* molecular dynamics for liquid metals. *Physical Review B* **47**, 558 (1993).
26. Kresse, G. & Furthmüller, J. Efficiency of *ab-initio* total energy calculations for metals and semiconductors using a plane-wave basis set. *Computational Materials Science* **6**, 15–50 (1996).

27. Kresse, G. & Furthmüller, J. Efficient iterative schemes for *ab-initio* total-energy calculations using a plane-wave basis set. *Physical Review B* **54**, 11169 (1996).
28. Kresse, G. & Joubert, D. From ultrasoft pseudopotentials to the projector augmented-wave method. *Physical Review B* **59**, 1758 (1999).
29. Perdew, J. P., Burke, K. & Ernzerhof, M. Generalized gradient approximation made simple. *Physical Review Letters* **77**, 3865 (1996).

Acknowledgements

The authors gratefully acknowledge support from the "Bundesministerium für Bildung und Forschung" (BMBF), and the computing time granted on Zentraleinrichtung für Datenverarbeitung (ZEDAT) at the Freie Universität Berlin. Also we thank Pouya Partovi-Azar for helpful discussions.

Author Contributions

S. Panahian Jand has analyzed the results and performed part of calculations. Q. Zhang has performed most of the calculations. P. Kaghazchi has analyzed the results and wrote the manuscript.

Additional Information

Competing Interests: The authors declare that they have no competing interests.

Publisher's note: Springer Nature remains neutral with regard to jurisdictional claims in published maps and institutional affiliations.